Shape-morphing architected sheets with non-periodic cut patterns

Paolo Celli, Connor Mcmahan, Brian Ramirez, Anton Bauhofer, Christina Naify, Douglas Hofmann, Basile Audoly, Chiara Daraio

Shape-Morphing Architected Sheets with Non-Periodic Cut Patterns

Paolo Celli[1,*], Connor McMahan[1], Brian Ramirez[1], Anton Bauhofer[1,2],
Christina Naify[3], Douglas Hofmann[3], Basile Audoly[1,4], Chiara Daraio[1,†]

[1]Department of Mechanical and Civil Engineering, California Institute of Technology, Pasadena, CA 91125, USA

[2]Department of Mechanical and Process Engineering, ETH Zurich, 8092 Zurich, Switzerland

[3]Jet Propulsion Laboratory/California Institute of Technology, Pasadena, CA, 91109, USA

[4]Laboratoire de Mécanique des Solides, CNRS, UMR 7649, École Polytechnique, 91128 Palaiseau CEDEX, France

* pcelli@caltech.edu, † daraio@caltech.edu

June 20, 2018

Abstract

Structuring geometrical features in a two-dimensional elastic sheet, which buckles in response to external actuation, allows faster and more scalable fabrication of three-dimensional objects. Here, we investigate the out-of-plane shape morphing capabilities of single-material elastic sheets with architected cut patterns. The sheets are laser-cut into an array of tiles connected by flexible hinges, which enable large deformations with small applied forces. We demonstrate that a non-periodic cut pattern can make a sheet buckle into selectable three-dimensional shapes, such as domes or patterns of wrinkles, when pulled at specific boundary points. These global buckling modes are observed in experiments, predicted by numerical simulations, and rationalized by a kinematic analysis that highlights the role of the geometric frustration arising from non-periodicity. The study focuses initially on elastic sheets, and is later extended to sheets made of elastic-plastic materials, which can retain their shape upon load removal. Our results provide a novel method for obtaining three-dimensional objects from initially-flat sheets by the application of tensile loads.

Imparting elastic sheets with a mesoscale architecture by folding [1, 2], perforating [3–5], or patterning them [6–8], enables the creation of materials with unusual characteristics, such as extreme extensibility [9], deployability [10, 11] and auxeticity [12]. These properties can be leveraged to design sheets that morph into complex three-dimensional objects. For example, origami sheets can be turned into nearly-arbitrary shapes [13, 14], but are typically challenging to fold [15] or actuate [16–18]. Patterned elastomeric sheets [6, 19], bilayers [20] and sheets with smart hinges [21–23] can morph into three-dimensional surfaces via non-mechanical stimuli, but their fabrication is complex. Ribbon- and membrane-like flat mesostructures, made of elastic or brittle materials, can buckle out of plane and produce three-dimensional geometries when subject to mechanical actuation in compression [24, 25] or tension [26, 27]. However,

compressive actuation requires pre-stretched substrates and non-trivial assembly processes, and the geometries obtained via tensile loads are limited to thin, arch-like features.

In contrast to shape-morphing origami or bilayer films, sheets with architected cut patterns can be easily fabricated via subtractive technologies. Their out-of-plane deformation can be triggered by manual forming [28, 29], via the actuation of smart hinges [30], or by applying compressive boundary loads [25, 31, 32]. Recently, it has been demonstrated that sheets with periodic perforations can also buckle locally in tension [27, 33–36], producing crease patterns that can be used for soft robotic locomotion [37] or as coatings for sunlight control [36]. However, since these buckling modes take place at the scale of the unit cells, the size of the transverse features they can produce cannot significantly exceed the typical length of the cuts. Non-periodic cut patterns have been seldom explored in this context: non-periodicity is known to lead to geometric frustration [38, 39], i.e., the desired deformation mode is impeded by the geometric incompatibility between neighboring cells. In the few cases where non-periodic cut patterns have been explored, frustration has been avoided [40–42]. In particular, the effect of geometric frustration on the out-of-plane deformations of thin architected sheets has been ignored so far.

In this work, we study the tensile response of elastic sheets featuring non-periodic cut patterns, and intentionally leverage geometric frustration to induce controllable, global shape changes via buckling. In most of our designs, we use point-like boundary loads that induce large deformations in selected sub-domains of the sheets. The inhomogeneous distribution of strains results into global buckling modes that make the sheets bend out of plane: we use this principle to obtain both dome-like surfaces, and patterns of wrinkles confined to pre-determined regions of the sheets. We show that the buckling pattern can be changed by applying the load at different points. We also extend the method to initially cylindrical—rather than planar—sheets and to cut patterns arranged into non-rectangular grids, and we demonstrate the formation of persistent three-dimensional surfaces by using sheets made of elastic-plastic materials [35].

We start by analyzing a simple cut pattern featuring a large-amplitude, planar mode of deformation. A 108-by-108 mm, 1.55 mm-thick natural rubber sheet is laser-cut [43] following a pattern of (*i*) diamond-shaped cut-outs and (*ii*) straight cut lines ending close to the diamonds' vertices. These two types of cuts are visible in black in the insets of Figure 1. The result is an array of 18×18 rhomboid tiles, visible in grey in the pictures, connected by thin hinges. The experimental traction curves (Figure 1) for unaxial tension reveal a strongly anisotropic and non-linear behavior (see the Experimental Section and SI Section S1 for details). When the tension is applied in the in-plane direction referred to as the x-direction (horizontal direction in the figure, black lines) the response is initially compliant up to a stretch value $\lambda \sim 1.3$, and then becomes much stiffer. When the tension is applied in the perpendicular y-direction (vertical direction in the figure, gray lines), the response is stiff and approximately linear for the range of stretch investigated; no initial compliant regime is observed. We simulated the mechanical response of the architected sheet numerically as well, by meshing a rectangular domain with periodic cut-outs, and by using a finite-element (FE) model for a neo-Hookean material in plane strain (the plane strain assumption is

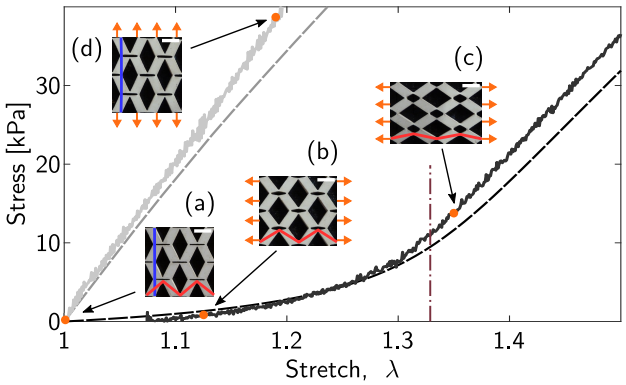

Figure 1: Uniaxial tension test of a periodic sheet whose undeformed geometry is shown in (a). The plot in the background shows the loading curve when the applied tension is either along the horizontal direction (black lines) or along the vertical direction (grey lines), both from experiments (solid lines) and from finite element simulations (dashed lines). The vertical dash-dot line shows the maximum stretch predicted by the kinematic analysis, where a geometric-to-elastic transition takes place. Insets (a-d) show snapshots of a 4×4-tile portion of the sheet at different levels of deformation (scale bar is 6 mm). The red and blue overlaid lines are obtained by joining the diagonals in a particular row and column of tiles, respectively, and are used to predict the maximum stretch by a kinematic analysis.

applicable as the in-plane width of the hinges is smaller than their out-of-plane thickness, see SI Section S2). The traction curves predicted by simulation are in good agreement with the experiments (Figure 1).

The salient features of the loading curves can be explained by a kinematic analysis, in which the sheet is modeled as an array of rigid tiles connected by pin joints. Such networks can feature modes of deformation known as *mechanisms* [44], which are mapped to low-energy configurations of the elastic sheet involving bending and shear [5] at the joints only. A mechanism relies on the coordinated rotation of the tiles in response to applied tension (Figure 1, SI Section S3 and [45, 46]). In particular, the maximum stretch attainable via a mechanism can be derived by a geometric argument, considering the broken lines connecting the diagonals of the tiles in a given row or column, see red and blue lines overlaid in Figure 1(a). As the length of these lines is preserved by mechanisms, the maximum stretch in the x or y direction is attained when the corresponding line is fully stretched out. For the cut design used in Figure 1, this maximum stretch is calculated by a geometric argument as $\lambda_x = 1.33$ in the x-direction, as indicated by the dash-dotted line in the figure; this is indeed where the compliant-to-stiff transition is observed in the experimental and numerical traction curves. For this particular cut design, the line of diagonals in the y-direction is already straight in the initial configuration, see the blue line in Figure 1(a), meaning that no mechanism can be activated when the tension is applied in the y-direction; this is consistent with the absence of an initial compliant regime in the grey curves in Figure 1.

Next, we introduce a family of periodic cut patterns parameterized by design variables. Our generic pattern, sketched in Figure 2(a), is obtained by cutting out diamonds with alternating directions, centered at the nodes of a grid of $N_x \times N_y$ rectangles, each with dimensions $l_x \times l_y$. The two families of diamonds are assigned different widths, w_x and w_y, so that the previous design comprising line-cuts can be recovered as the special case $w_y = 0$. The length of the diamonds is such that a gap (hinge) of width δ is present between adjacent diamonds. Three

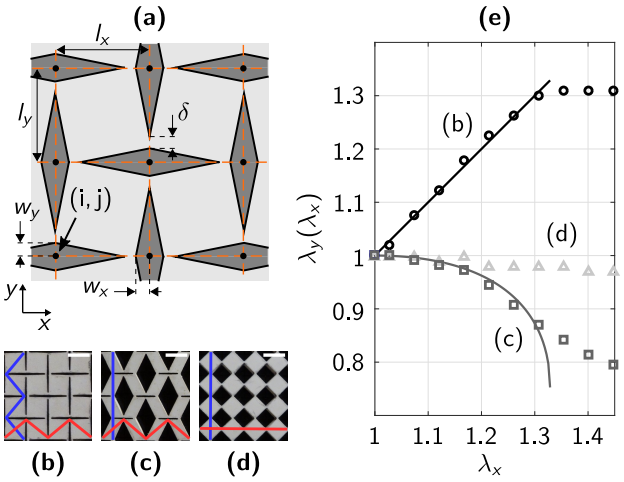

Figure 2: (a) Sketch of a generic periodic architecture parameterized by design variables. (b-d) Digital images of details of three periodic undeformed specimens, corresponding to different values of (w_x, w_y) listed in Section S4 in the SI; scale bar is 6 mm. (e) Transverse stretch λ_y as a function of the axial stretch λ_x for simple traction along the x-direction, and for the same set of specimens: experiments (open symbols) versus preditions of the kinematic model (solid curves).

examples of periodic geometries cut out in natural rubber sheets are shown in Figure 2(b-d), for $N_x = N_y = 18$, $l_x = l_y = 6\,\text{mm}$, and out-of-plane thickness $t = 1.55\,\text{mm}$; note that the shape of the tiles, shown in light grey, can now vary from rhomboid to square. Experimental traction curves for three particular cutting patterns are plotted in the plane of stretches (λ_x, λ_y) in Figure 2(e), and compared with the predictions of the kinematic analysis (see SI Section S3 for a detailed derivation),

$$\lambda_y\left(\lambda_x\right) = \frac{d_v}{l_y}\,\sin\left[\gamma + \arccos\left(\frac{\lambda_x l_x}{d_h}\right)\right]\,, \tag{1}$$

where $d_h = \sqrt{l_x^2 + [l_y - 2w_y - \delta]^2}$ and $d_v = \sqrt{l_y^2 + [l_x - 2w_x - \delta]^2}$ are the lengths of the diagonals of a tile, and γ is the angle between these diagonals. The design variables have a strong influence on tension tests. The cut pattern in Figure 2(b) gives rise to an auxetic mechanism [12] having a negative Poisson's ratio $\nu = -1$; this is reflected by the positive slope of the black curve in Figure 2(d). By contrast, the mechanism associated with the cut pattern in Figure 1 and 2(c) has a positive Poisson's ratio. For both these cut patterns, the kinematic model in Equation (1) provides an accurate prediction of the transverse stretch $\lambda_y(\lambda_x)$ up to around $\lambda_x \sim 1.3$, where the joints start to stretch, see Figure 2(e). Finally, the cut pattern in Figure 2(d) is stiff when loaded in tension since the maximum stretch $\lambda_x = 1$ predicted by the kinematic analysis is attained in the undeformed configuration (the diagonals of adjacent tiles are aligned). The effect of the design parameters δ and t on the in-plane response is investigated in the SI, Section S5.

Having analyzed a family of *periodic* cut patterns parameterized by the design variables w_x and w_y, we now investigate *non-uniform* designs, obtained by specifying arbitrary values of w_x and w_y in every cell of a rectangular grid; the cell size $l_x \times l_y$ is uniform throughout the sheet. Upon deformation, we expect that every unit cell of these

non-periodic sheets will try to follow the mechanism corresponding to the local values of w_x and w_y, as described by Equation (1). However, mechanisms corresponding to neighboring cells are not geometrically compatible in general (see SI Section S3). Thus, we investigate how this incompatibility is resolved at the global level by buckling. As a first example, we consider a cut geometry where w_x is constant while w_y varies sinusoidally in the y-direction, see Figure 3(a1), using a 1.55 mm-thick natural rubber sheet with $N_x = 36$, $N_y = 18$, $l_x = 6\,\text{mm}$, $l_y = 2\,l_x$. This

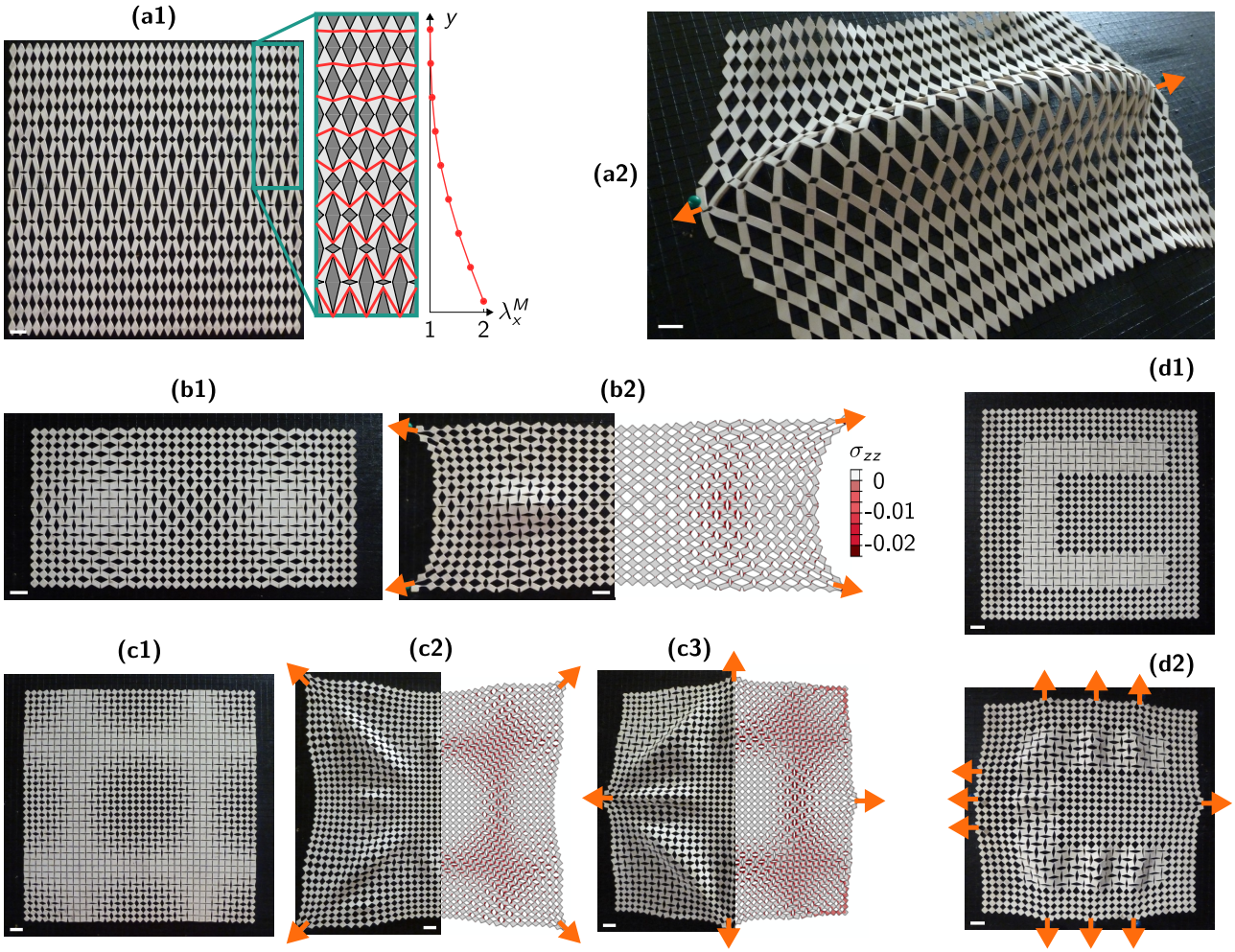

Figure 3: Out-of-plane morphing of sheets with non-periodic cut patterns. (a1) Cut pattern with gradient in the y direction. The inset to the right of the undeformed configuration highlights the tile diagonals (in red), that are inextensible by the local kinematic analysis, as well as a plot of the corresponding maximum stretch $\lambda_x^M(y)$: this shows that the sheet is highly stretchable in the center, but inextensible along its upper and lower edges. (a2) A dome shape obtained when the sheet is pulled from two boundary points. (b1) Undeformed configuration of a specimen featuring two soft and auxetic regions in its interior, which give rise to two localized bumps upon pulling at the four corners (b2). (c1-c3) Undeformed and deformed configurations of another specimen, highlighting the influence of the boundary loading on the pattern of wrinkles. The right-halves of (b2), (c2) and (c3) are the stress maps of $\sigma_{zz} = \nu(\sigma_{xx} + \sigma_{yy})$ (under the plane strain assumption); negative values of the average in-plane stress $(\sigma_{xx} + \sigma_{yy})$ are taken as an indicator for buckling. (d1-d2) Shaping wrinkles: a C-shaped soft and auxetic region is embedded in a sheet by a suitable choice of the maps of w_x and w_y in the reference configuration (d1). The wrinkles localize upon the application of boundary loads (d2). The orange arrows indicate the boundary loads. Scale bar: 12 mm.

choice of maps for w_x and w_y ensures that the top and bottom parts of the sheet are virtually undeformable, see

the inset in Fig. 3(a1), while the center is highly stretchable. When the sheet is stretched by point-like forces, as in Figure 3(a2), the strong geometric incompatibility between the center and the edges produces a global buckling mode spanning the central region. Note that this buckling instability takes place in tension, unlike in the classical Euler buckling. For a given cut pattern, the dependence of the buckled configuration on the sheet's thickness t is similar to what can be expected from the classical theory of plates without cut-outs, see Section S6 for details. As t increases, the onset of buckling occurs at larger critical stretches, consistent with the fact that the effective bending modulus is larger. An increased thickness also yields larger deflections and makes the buckling pattern spread further away from the the line of application of the force.

More complex buckling patterns can be obtained by letting both w_x and w_y vary along the sheet, either smoothly or abruptly. As an example, we study a sheet comprising two stretchable and auxetic islands surrounded by unstretchable and non-auxetic regions, see Figure 3(b1). This geometry induces strong geometric incompatibilities: when the sheet is stretched, the auxetic islands tend to swell in the transverse direction. This swelling is prevented by the surrounding stiff regions, and compressive in-plane stress appears, as confirmed by the FE simulations in Figure 3(b2). Ultimately, this leads to a buckling pattern made up of two domes localized on the auxetic islands, see Figure 3(b2). As another example, we study the response of a sheet with a more complex cut pattern obtained by varying both w_x and w_y sinusoidally along both the horizontal and vertical directions. The experimental results in (c2) and (c3), corresponding to actuation at the structures' corners or boundary mid-points, respectively, show markedly different wrinkle patterns, thereby highlighting the role of the applied force in selecting the pattern. Finally, in Figure 3(d1-d2), we show the response of a sheet featuring a C-shaped auxetic region separated from the rest of the sheet, which is unstretchable, by a sharp boundary. In this case, pulling the specimen as indicated by the orange arrows leads to wrinkles localized along the C-like domain. The wavelength of the wrinkles is comparable to the width of the C-shaped domain. These examples show that the buckling patterns can be tailored by engineering the sheet's local properties through the maps of w_x and w_y, and by choosing the points of application of the load.

Our approach can be extended to solids of revolution. For example, we pattern a sheet by varying w_x and w_y in vertical stripes, alternating regions of auxetic and not-auxetic behavior. We then roll the sheet, forming a tube, and pull on its ends. The applied tractions force the tube to expand at prescribed, auxetic sections and to contract at others [47], see Figure 4(a). Stretching the tube further produces a non-axisymmetric buckling bifurcation, with an azimuthal wavelength roughly comparable to the stripes' width. Cut patterns can also be attached to non-Cartesian grids, as illustrated in the example in Figure 4(b), where the petal-like sheet closes up into a pea pod shape when pulled at its ends.

The design strategy is not limited to elastic materials such as rubber. Permanent three-dimensional shapes can be obtained by using an elastic-plastic material [35]. This requires modifying the hinge design to avoid breakage: the new design, shown in the insets in Figure 4(c), was inspired by [48] and is discussed in SI Section S7. The deformation of two sheets featuring the same initial cut pattern, one made of natural rubber and one made of

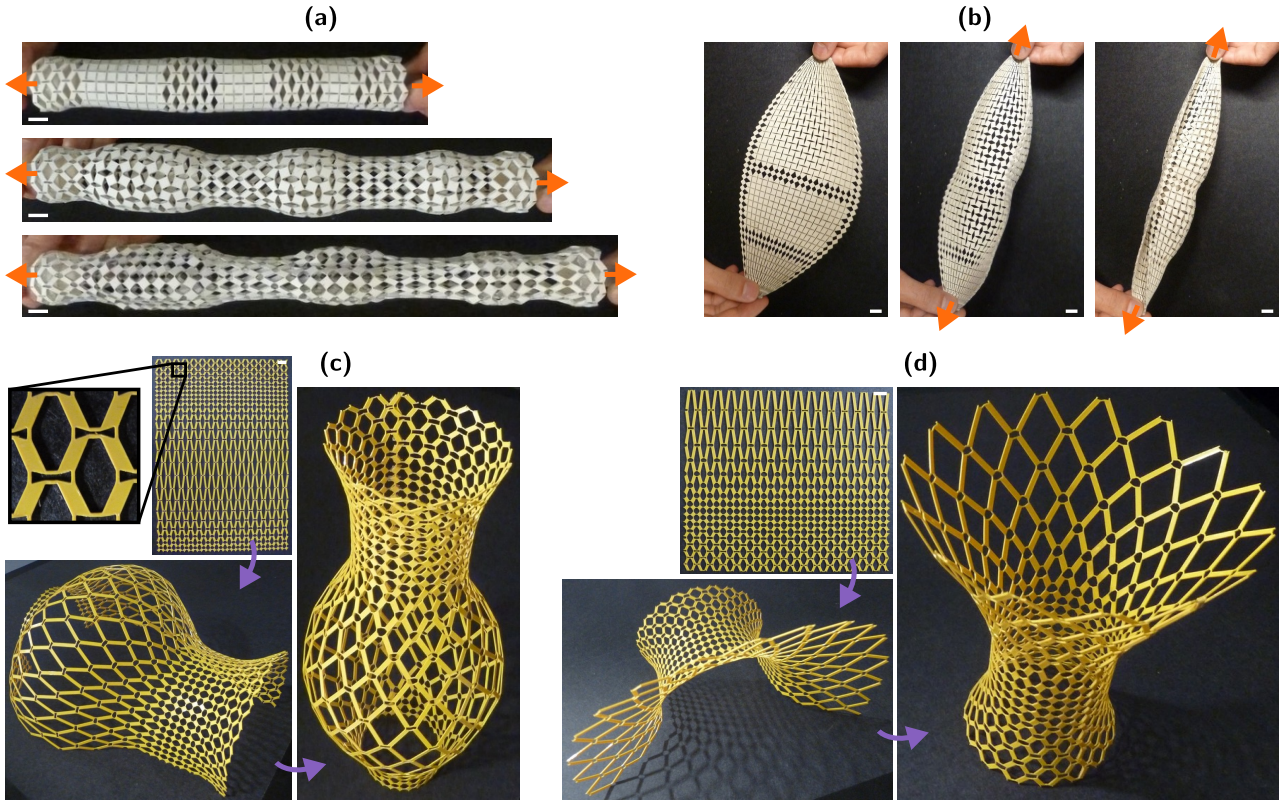

Figure 4: (a) An architected tube can expand or contract radially based on an initial stripe pattern. Beyond a critical tensile load, an azimuthal buckling pattern appears in the expanded regions. (b) Petal-shaped specimen generated from a non-rectangular grid. This sheet morphs into a pea pod-shaped object when pulled from its ends. (c-d) Sculpting axisymmetric shapes from a sheet made of an elastic-plastic material; the shapes are obtained by using graded cut patterns and by stretching out the sheets locally by hand. Scale bars: 12 mm.

stiff PETG are compared in Figure S12. While they feature a similar buckling pattern, the second sheet deforms irreversibly, leaving a permanent pattern after load removal. We leverage the elastic-plastic behavior to sculpt axisymmetric shapes out of a planar PETG sheet, see Figure 4(c-d). As earlier with the tube, the cut patterns are graded along the axis, which allows us to select the radial expansion (hence the target radius) as a function of the axial coordinate. To obtain an even larger stretchability contrast, we use non-regular rectangular grids, i.e., we set $l_y(y)$ to take on larger values in the regions of large stretch. The irreversible deformations are obtained by stretching the sheet locally by hand, and a similar effect could be achieved using localized smart-material actuators or pressurized membranes. These structures are reminiscent of gridshells [49] and are easier to fabricate, especially at small scales.

In this work, we have demonstrated that geometric incompatibility can be leveraged to create three-dimensional objects from sheets with non-periodic cut-outs. By choosing the properties of the cuts locally, one can prescribe a map of maximum stretch, which is resolved when the sheet bends out of plane in response to boundary loads or local stretching. While the shapes we have obtained are relatively simple, these design principles could be extended to different families of mechanisms, and could be coupled to optimization and inverse-design strategies to obtain more complex shapes. Due to the flexibility of the fabrication process, which involves cutting mono-layer sheets,

this approach could be used to produce three-dimensional structures at vastly different scales.

Experimental Section

Specimen fabrication. A Universal ILS9 120W laser cutter is used to create perforations. We mainly use 1.55 mm-thick natural rubber sheets (McMaster-Carr, item no. 8633K71), but some 3.1 mm- and 0.75 mm-thick ones were also used (Grainger, items no. 1XWE5 and 8611K18). For the 1.55 mm-thick specimens, the machine is set to cut at 35% power and 5% speed, with an air assist flow rate of 100% to avoid burning the specimens. For the 3.1 mm-thick specimens, 45% power and 2.3% speed are selected. For the 0.75 mm-thick specimens, 30% power and 5% speed are selected. Since the laser beam has a finite cutting diameter, the hinges are not characterized by sharp corners but are de-facto beams having a finite length. The tube specimens are closed using double-sided tape glued to some tiles. PETG sheets (0.5 mm-thick) were perforated with the same laser cutter, with 3.0% power and 2.2% speed, and were also closed into surfaces of revolution using double-sided tape.

Material testing. Uniaxial tensile tests are conducted using an Instron ElectroPuls (Model E3000) system equipped with a 250 N load cell at a constant deformation rate of $2\,\mathrm{mm\,s^{-1}}$. The specimens are stretched by pulling on some of the hinges using a customized fixture which allows for lateral expansion or contraction of the sheets being pulled (see SI Section S1). The tensile forces and displacements are measured with 1 mN and 5 μm accuracy, respectively, at an acquisition rate of 1 kHz. The force-displacement data obtained from the Instron WaveMatrix software is converted to stress-stretch data using the original sample dimensions. The data obtained is then subsampled to remove some of the noise (one every 10 measurements is kept). Finally, the stretch is adjusted to account for the self-weight elongation experienced by some specimens featuring a pronounced mechanism-like behavior along the direction parallel to the load.

Supporting Information

Supporting Information is available in tail of this manuscript.

Acknowledgements

This research was carried out at the California Institute of Technology and the Jet Propulsion Laboratory under a contract with the National Aeronautics and Space Administration, and funded through the President's and Director's Fund Program. This work is partially supported through the Foster and Coco Stanback Space Innovation Fund. P.C. wishes to thank D. Pasini of McGill University for useful suggestions, A. Constantinescu of École Polytechnique, and members of C.D.'s research group at Caltech for their input and suggestions. We also thank B.

Dominguez of Caltech for his assistance during laser cutting.

References

[1] M. Schenk, S. D. Guest. *Proc. Natl. Acad. Sci. U.S.A.* **2013**, *110*, 9 3276.

[2] J. L. Silverberg, A. A. Evans, L. McLeod, R. C. Hayward, T. Hull, C. D. Santangelo, I. Cohen. *Science* **2014**, *345*, 6197 647.

[3] T. Mullin, S. Deschanel, K. Bertoldi, M. C. Boyce. *Phys. Rev. Lett.* **2007**, *99* 084301.

[4] D. M. Sussman, Y. Cho, T. Castle, X. Gong, E. Jung, S. Yang, R. D. Kamien. *Proc. Natl. Acad. Sci. U.S.A.* **2015**, *112*, 24 7449.

[5] C. Coulais, C. Kettenis, M. van Hecke. *Nat. Phys.* **2017**, *14* 40.

[6] J. Kim, J. A. Hanna, M. Byun, C. D. Santangelo, R. C. Hayward. *Science* **2012**, *335*, 6073 1201.

[7] Q. Ge, H. J. Qi, M. L. Dunn. *Appl. Phys. Lett.* **2013**, *103*, 13 131901.

[8] A. S. Gladman, E. A. Matsumoto, R. G. Nuzzo, L. Mahadevan, J. A. Lewis. *Nat. Mater.* **2016**, *15* 413.

[9] Y. Tang, J. Yin. *Extreme Mech. Lett.* **2017**, *12* 77.

[10] E. T. Filipov, T. Tachi, G. H. Paulino. *Proc. Natl. Acad. Sci. U.S.A.* **2015**, *112*, 40 12321.

[11] J. T. B. Overvelde, J. C. Weaver, C. Hoberman, K. Bertoldi. *Nature* **2017**, *541* 347.

[12] J. N. Grima, V. Zammit, R. Gatt, A. Alderson, K. E. Evans. *Phys. Status Solidi B* **2007**, *244*, 3 866.

[13] L. H. Dudte, E. Vouga, T. Tachi, L. Mahadevan. *Nat. Mater.* **2016**, *15* 583.

[14] S. J. P. Callens, A. A. Zadpoor. *Mater. Today* **2018**, *21*, 3 241.

[15] E. D. Demaine, T. Tachi. In *33rd Int. Symp. on Comput. Geom. (SoCG 2017)*, volume 77. **2017** 34:1–34:16.

[16] E. Hawkes, B. An, N. M. Benbernou, H. Tanaka, S. Kim, E. D. Demaine, D. Rus, R. J. Wood. *Proc. Natl. Acad. Sci. U.S.A.* **2010**, *107*, 28 12441.

[17] M. Stern, M. B. Pinson, A. Murugan. *Phys. Rev. X* **2017**, *7* 041070.

[18] P. Plucinsky, B. A. Kowalski, T. J. White, K. Bhattacharya. *Soft Matter* **2018**, *14* 3127.

[19] T. H. Ware, M. E. McConney, J. J. Wie, V. P. Tondiglia, T. J. White. *Science* **2015**, *347*, 6225 982.

[20] W. M. van Rees, E. Vouga, L. Mahadevan. *Proc. Natl. Acad. Sci. U.S.A.* **2017**, *114*, 44 11597.

[21] S. M. Felton, M. T. Tolley, B. Shin, C. D. Onal, E. D. Demaine, D. Rus, R. J. Wood. *Soft Matter* **2013**, *9* 7688.

[22] J. H. Na, A. A. Evans, J. Bae, M. C. Chiappelli, C. D. Santangelo, R. J. Lang, T. C. Hull, R. C. Hayward. *Adv. Mater.* **2014**, *27*, 1 79.

[23] S. Ahmed, Z. Ounaies, M. Frecker. *Smart Mater. Struct.* **2014**, *23*, 9 094003.

[24] S. Xu, Z. Yan, K. Jang, W. Huang, H. Fu, J. Kim, Z. Wei, M. Flavin, J. McCracken, R. Wang, A. Badea, Y. Liu, D. Xiao, G. Zhou, J. Lee, H. U. Chung, H. Cheng, W. Ren, A. Banks, X. Li, U. Paik, R. G. Nuzzo, Y. Huang, Y. Zhang, J. A. Rogers. *Science* **2015**, *347*, 6218 154.

[25] Y. Zhang, Z. Yan, K. Nan, D. Xiao, Y. Liu, H. Luan, H. Fu, X. Wang, Q. Yang, J. Wang, W. Ren, H. Si, F. Liu, L. Yang, H. Li, J. Wang, X. Guo, H. Luo, L. Wang, Y. Huang, J. A. Rogers. *Proc. Natl. Acad. Sci. U.S.A.* **2015**, *112*, 38 11757.

[26] M. A. Dias, M. P. McCarron, D. Rayneau-Kirkhope, P. Z. Hanakata, D. K. Campbell, H. S. Park, D. P. Holmes. *Soft Matter* **2017**, *13* 9087.

[27] X. Guo, X. Wang, D. Ou, J. Ye, W. Pang, Y. Huang, J. Rogers, Y. Zhang. *npj Flexible Electron.* **2018**, *2* 14.

[28] M. Konaković, K. Crane, B. Deng, S. Bouaziz, D. Piker, M. Pauly. *ACM Trans. Graph.* **2016**, *35*, 4 89.

[29] F. Wang, X. Guo, J. Xu, Y. Zhang, C. Q. Chen. *J. Appl. Mech.* **2017**, *84*, 6 061007.

[30] J. Cui, J. G. M. Adams, Y. Zhu. *Smart Mater. Struct.* **2017**, *26*, 12 125011.

[31] R. M. Neville, F. Scarpa, A. Pirrera. *Sci. Rep.* **2016**, *6* 31067.

[32] H. Fu, K. Nan, W. Bai, W. Huang, K. Bai, L. Lu, C. Zhou, Y. Liu, F. Liu, J. Wang, M. Han, Z. Yan, H. Luan, Y. Zhang, Y. Zhang, J. Zhao, X. Cheng, M. Li, J. W. Lee, Y. Liu, D. Fang, X. Li, Y. Huang, Y. Zhang, J. A. Rogers. *Nat. Mater.* **2018**, *17* 268.

[33] M. K. Blees, A. W. Barnard, P. A. Rose, S. P. Roberts, K. L. McGill, P. Y. Huang, A. R. Ruyack, J. W. Kevek, B. Kobrin, M. D. A., P. L. McEuen. *Nature* **2015**, *524* 204.

[34] T. C. Shyu, P. F. Damasceno, P. M. Dodd, A. Lamoreaux, L. Xu, M. Shlian, M. Shtein, S. C. Glotzer, N. A. Kotov. *Nat. Mater.* **2015**, *14* 785.

[35] A. Rafsanjani, K. Bertoldi. *Phys. Rev. Lett.* **2017**, *118* 084301.

[36] Y. Tang, G. Lin, S. Yang, Y. K. Yi, R. D. Kamien, J. Yin. *Adv. Mater.* **2017**, *29*, 10 1604262.

[37] A. Rafsanjani, Y. Zhang, B. Liu, S. M. Rubinstein, K. Bertoldi. *Sci. Rob.* **2018**, *3*, 15.

[38] C. Coulais, E. Teomy, K. de Reus, Y. Shokef, M. van Hecke. *Nature* **2016**, *535* 529.

[39] R. Guseinov, E. Miguel, B. Bickel. *ACM Trans. Graph.* **2017**, *36*, 4 64.

[40] Y. Cho, J.-H. Shin, A. Costa, T. A. Kim, V. Kunin, J. Li, S. Y. Lee, S. Yang, H. N. Han, I.-S. Choi, D. J. Srolovitz. *Proc. Natl. Acad. Sci. U.S.A.* **2014**, *111*, 49 17390.

[41] A. Ion, J. Frohnhofen, L. Wall, R. Kovacs, M. Alistar, J. Lindsay, P. Lopes, H.-T. Chen, P. Baudisch. In *UIST '16*. ISBN 978-1-4503-4189-9, **2016** 529–539.

[42] M. J. Mirzaali, S. Janbaz, M. Strano, L. Vergani, A. A. Zadpoor. *Sci. Rep.* **2018**, *8* 965.

[43] A. Rafsanjani, D. Pasini. *Extreme Mech. Lett.* **2016**, *9* 291.

[44] S. Pellegrino, C. Calladine. *Int. J. Solids Struct.* **1986**, *22*, 4 409.

[45] R. G. Hutchinson, N. A. Fleck. *J. Mech. Phys. Solids* **2006**, *54*, 4 756.

[46] V. Kapko, M. M. J. Treacy, M. F. Thorpe, S. D. Guest. *Proc. Royal Soc. A* **2009**, *465*, 2111 3517.

[47] J. Liu, Y. Zhang. *Soft Matter* **2018**, *14* 693.

[48] X. Shang, L. Liu, A. Rafsanjani, D. Pasini. *J. Mater. Res.* **2018**, *33*, 3 300.

[49] C. Baek, A. O. Sageman-Furnas, M. K. Jawed, P. M. Reis. *Proc. Natl. Acad. Sci. U.S.A* **2018**, *115*, 1 75.